metals

MDPI

Article

Feasibility Study on the Fabricating of Carbon-Nanotube-Reinforced Al-Si-Cu Alloy Matrix Composites Using Oxygen-Replacing Die Casting Process

Seong-Hyo Oh [1,2], Ho-Jung Kang [1,2], Pil-Hwan Yoon [1], Gyu-Heun Lee [1], Sun-Mi Shin [1], Yoon-Suk Choi [2,*] and Jin-Young Park [1,*]

[1] Advanced Forming Process R&D Group, Korea Institute of Industrial Technology, Ulsan 44776, Republic of Korea; osh3274@kitech.re.kr (S.-H.O.); hjkang7@kitech.re.kr (H.-J.K.); ph1047@kitech.re.kr (P.-H.Y.); leegh1@kitech.re.kr (G.-H.L.); smshin@kitech.re.kr (S.-M.S.)
[2] Department of Material Science and Engineering, Pusan National University, Busan 46200, Republic of Korea
* Correspondence: choiys@pusan.ac.kr (Y.-S.C.); jpark7@kitech.re.kr (J.-Y.P.); Tel.: +82-52-980-7735 (J.-Y.P.); Fax: +82-52-980-7799 (J.-Y.P.)

Abstract: A383 Al-Si-Cu alloy matrix composites were reinforced with different amounts (0.5, 1.0, 1.5 and 2.0 wt%) of chopped multiwalled carbon nanotubes (MWCNTs) and fabricated using the oxygen-replacing die casting (ORDC) process to reduce gas porosities via the reaction of molten Al and O_2 replaced in the mold cavity. MWCNTs were added to the mold cavity by supplying O_2 and using a poly gate in the ORDC mold to improve CNT dispersity in the matrix of the composite. Microstructure studies of the composites showed a uniform CNT distribution within the matrix and grain refinement. X-ray computed tomography images showed that the internal porosities were affected by the CNT addition amount and gate type used in the mold, and Raman spectroscopy analysis indicated that CNTs in the matrix were free of significant defects. The 1.0 wt% CNT-added composite cast using the poly gate showed the highest ultimate tensile strength of 258.5 ± 5.2 MPa and hardness of 157.9 ± 3.0 Hv; these values were, respectively, 21% and 30% higher than those of the monolithic A383 alloy, confirming the feasibility of fabricating the MWCNT-added A383 alloy composite with a poly gate using the ORDC process.

Keywords: multiwalled carbon nanotubes (MWCNTs); MWCNTs-reinforced A383 Al-Si-Cu alloy matrix composite; oxygen-replacing die casting (ORDC); single gate; poly gate; CNT distribution; Al_2O_3 phase; grain refinement; internal porosity; mechanical properties

check for updates

Citation: Oh, S.-H.; Kang, H.-J.; Yoon, P.-H.; Lee, G.-H.; Shin, S.-M.; Choi, Y.-S.; Park, J.-Y. Feasibility Study on the Fabricating of Carbon-Nanotube-Reinforced Al-Si-Cu Alloy Matrix Composites Using Oxygen-Replacing Die Casting Process. *Metals* **2023**, *13*, 730. https://doi.org/10.3390/met13040730

Received: 10 March 2023
Revised: 31 March 2023
Accepted: 6 April 2023
Published: 8 April 2023

Copyright: © 2023 by the authors. Licensee MDPI, Basel, Switzerland. This article is an open access article distributed under the terms and conditions of the Creative Commons Attribution (CC BY) license (https://creativecommons.org/licenses/by/4.0/).

1. Introduction

Al-Si casting alloys are medium strength materials and have been widely used for manufacturing light-weight automobile components. However, the extent to which their characteristics such as high strength can be improved is limited. To overcome this limit, studies have been investigating fabricating composites with existing Al casting alloys [1–3]. Carbon nanotubes (CNTs) are well known to offer excellent mechanical strength and thermal conductivity as a reinforcement for composite materials [4–8]. Accordingly, studies have investigated various methods for fabricating CNT-reinforced metal matrix composites (MMCs) such as powder metallurgy (PM), stir casting, electrochemical methods and CNT coating, etc. However, existing composite fabrication technologies are not sufficiently reliable [9–14]. In particular, CNTs suffer deterioration when they make contact with molten Al, and they have poor dispersity owing to the low wettability caused by the high surface tension of aluminum; these are the most challenging outstanding problems [15–17]. Larianovsky et al. developed and evaluated a high-pressure die casting (HPDC) process followed by several cyclic extrusions for producing Al/CNT composites by the direct

injection of CNTs into pure Al. They mentioned that the short solidification time during HPDC prevents CNT damage and aluminum carbide formation at CNT/Al interfaces [18].

The A383 alloy is the most representative casting alloy for the HPDC process due to its excellent characteristics such as high strength, high fluidity and high corrosion resistance [19]. Therefore, it has been widely used in manufacturing automotive castings such as the engine block, cylinder head case and oil pan [20]. Moreover, HPDC has been also widely applied to cast automobile components because it effectively enables mass-production by rapid molten metal injection into a mold cavity and affords excellent dimensional accuracy [21,22]. However, it has been limited in its application to automobile body parts requiring high strength because air entrapped in the molten metal during injection causes porosity defects. To reduce the production of porosity defects in this die-casting process, alternative casting method such as the oxygen-replacing die casting (ORDC) process have been investigated. In this process, oxygen is supplied into the mold cavity to replace the inner air (mainly N_2) before molten Al is injected to form Al_2O_3 through a chemical reaction with the O_2 gas (Equation (1)); therefore, O_2 consumption ultimately suppresses porosity defects inside the casting [23–25]. In addition to the reduced porosity defects, ORDC is also known to have the advantages of the dispersion strengthening effect of Al_2O_3 particles and further improving filling via heat generation during the reaction while maintaining the high productivity and high dimensional accuracy of the HPDC process [26,27].

$$2Al(molten) + 3/2O_2(gas) = Al_2O_3 \quad (1)$$

In this study, we evaluated the feasibility of fabricating the CNT-reinforced A383 alloy matrix composite by using ORDC through the adding of CNTs into the mold cavity using an O_2 gas supply. Theoretically, successful fabrication of the CNT-reinforced Al matrix composite is expected with the following conditions: good CNT distribution in the matrix by CNT addition using the oxygen supplying process, increased numerous Al_2O_3 formation by improved reaction between the molten Al metal and oxygen gas by using poly gates, avoiding CNT deterioration by having a very short exposing time by using rapid filling and solidification of the ORDC process, and reduced porosities. Furthermore, the CNT-reinforced A383 alloy composites produced using the ORDC process have the potential to fabricate large-sized and complex-shaped parts such as automobile body parts which require a light-weight and high strength while maintaining the high productivity of the conventional ORDC process. Moreover, the ORDC process is very competitive when compared to other fabricating methods such as PM and the casting method with CNT-inserted molten metal, etc.

2. Materials and Methods

SEM micrographs of the as-received multiwalled carbon nanotubes (MWCNTs) and MWCNTs used as reinforcements in the present study are shown in Figure 1. The as-received MWCNTs (Figure 1a,b) had an average length of 100 μm and diameter of 20–30 nm. They were chopped into smaller lengths of 5–10 μm (Figure 1c,d) as this was expected to improve the CNT dispersity in the matrix [28,29]. Chopped MWCNTs had a purity of >95 wt%, tap density of 0.28 g/cm^3 and electrical conductivity of >100 S/cm.

The A383 aluminum alloy was used as the matrix alloy; its chemical composition is listed in Table 1.

Table 1. Chemical composition (wt%) of A383 alloy used as the matrix alloy.

Si	Cu	Zn	Fe	Mg	Mn	Ti	Pb	Al
11.72	1.93	0.918	0.726	0.206	0.197	0.045	0.038	Bal.

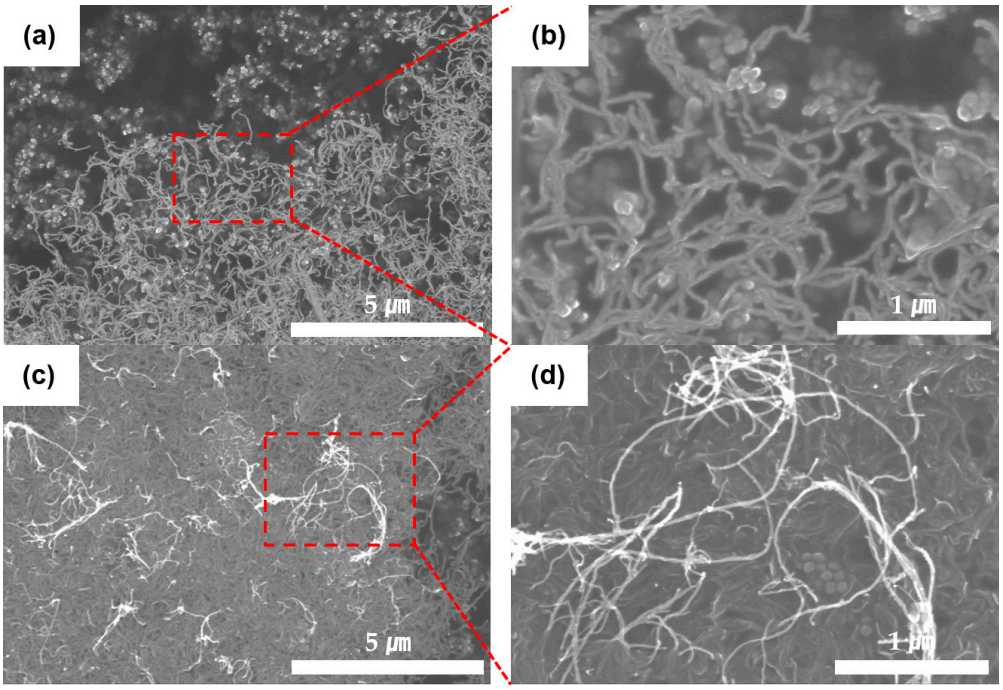


Figure 1. SEM micrographs of (**a**,**b**) as-received MWCNTs (length: 100 μm) and (**c**,**d**) chopped MWCNTs (length: 5–10 μm).

Figure 2 shows a schematic of the experimental setup used for the fabrication of the composites using ORDC. It consisted of the mold with the cavity, gate and runner part, and O_2-supplying system connected to the sleeve with the pouring inlet [23,24]. A container attached to the O_2-supplying tube supplied CNTs via the Venturi effect when O_2 was supplied.

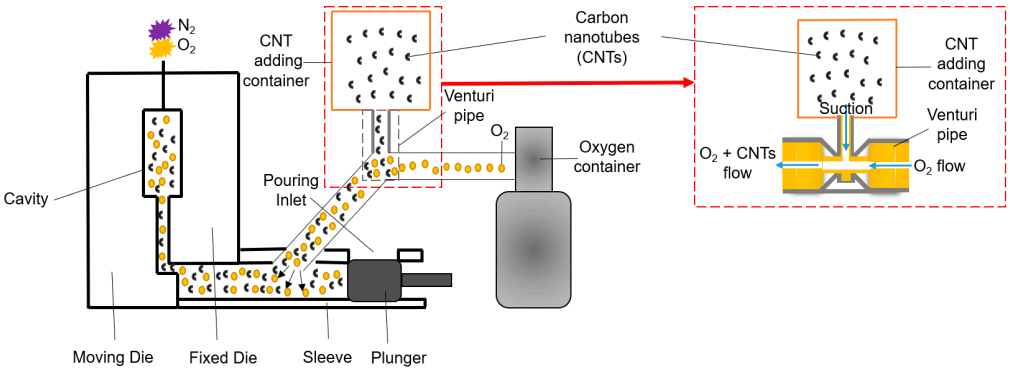


Figure 2. Schematic of experimental setup for fabricating composites using ORDC with CNT-adding system.

A schematic of the casting design of the mold is shown in Figure 3. It consists of the cavity part that produces the cast product, runner, overflow and gate part (Figure 3a). In the present study, two types of gate were designed: a single gate (one entrance with a rectangular shape) and a poly gate (multiple entrances with a triangular shape) (Figure 3b).

The composites were fabricated using the following procedure. Approximately 150 kg of the A383 alloy was melted at 680 °C in an electrical resistance furnace. Gas bubbling filtration (FS Korea, Ulsan, Republic of Korea) was performed for 8 min at 300 rpm to improve the purity of the molten alloy. The casting was performed by using a 125-ton cold-chamber die casting machine (TOYO, TOYO125, Ulsan, Republic of Korea). The plunger in the sleeve blocked the molten metal inlet, and then 1.26 L of O_2 (purity: 99.99%) was supplied for 2.5 s at 5 bar to replace the inner air (mostly N_2 gas), as these were reported

as the optimal conditions for the ORDC process [24]. As the air in the mold cavity and sleeve was fully replaced with O_2, various amounts (0.5, 1.0, 1.5 and 2.0 wt%) of CNTs were added into the cavity and sleeve via the Venturi effect produced by the O_2 supply pressure. After that, the plunger blocking the molten metal inlet was retreated and the molten Al was poured in the sleeve. The O_2 supply was stopped and the plunger moved to inject molten Al into the mold under various casting conditions, as noted in Table 2. As a reference process for comparison with the ORDC process, the conventional HPDC process was performed with the monolithic A383 alloy without added CNT.

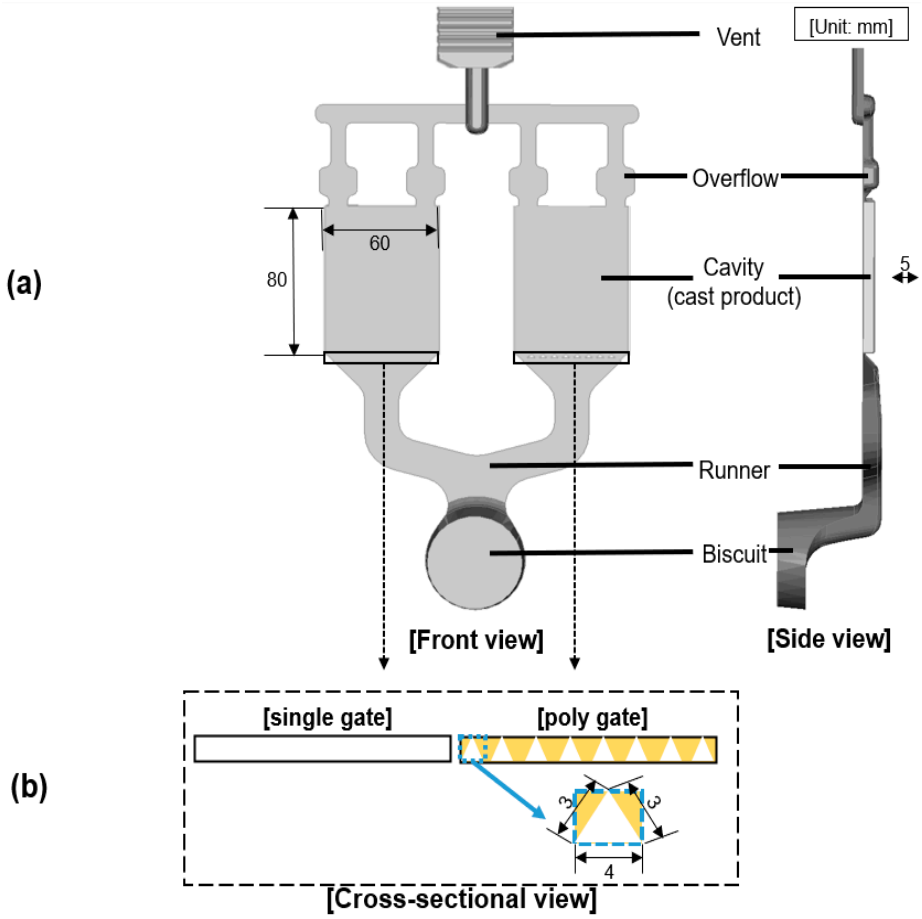


Figure 3. Schematic of casting design of mold: (**a**) front and side views of casting design and (**b**) cross-sectional view of single gate and poly gate of mold.

The microstructures of the samples were examined using optical microscopy (Olympus BX51, Ulsan, Republic of Korea), scanning electron microscopy (SEM; Hitachi, SU8020, Ulsan, Republic of Korea) and high-resolution transmission electron microscopy (HR-TEM; JEOL, JEM-2100F, Ulsan, Republic of Korea). To analyze the characteristics of the precipitates and CNTs in the composites, X-ray diffraction (XRD; ULTIMA4, Rigaku, Ulsan, Republic of Korea) and confocal Raman spectroscopy (WITec, alpha300R, Ulsan, Republic of Korea) were used, respectively. The internal porosity of the samples was evaluated using X-ray computed tomography (CT; Nikon, XTH320L, Ulsan, Republic of Korea) [23,24]. To evaluate the mechanical properties of the samples, the tensile strength was evaluated (Instron, 5989, Ulsan, Republic of Korea); a hardness test (Matsuzawa, PMT-X7, Ulsan, Republic of Korea) and fractographic examination were performed on the tensile test specimens [30–32].

Table 2. Casting conditions of HPDC and ORDC processes.

Parameters		HPDC	ORDC				
Added amount of CNTs (wt%)		0	0	0.5	1.0	1.5	2.0
Molten metal pouring temp. (°C)		680					
Preheated mold temp. (°C)		200					
Casting pressure (MPa)		80					
Filling rate of sleeve (%)		32					
Biscuit thickness (mm)		20					
Plunger velocity (m/s)	low	$0.1 \rightarrow 0.2 \rightarrow 0.25$					
	high	1.5					
Stroke with high velocity (mm)		66 (total stroke: 256)					

3. Results and Discussion

3.1. Microstructural Observation of CNT-Added A383 Composite

Figure 4 shows images of the as-cast A383 alloy and CNT-added composites cast using a single gate and poly gate. The as-cast state consisted of cavities (places where the composites were cast), a runner, vent, overflow, gates and biscuit. Few casting defects such as misrun, soldering and cracks are seen in Figure 4b. Furthermore, compared to the product cast using a single gate (Figure 4a), that cast using a poly gate (Figure 4c) shows several distinct melt flow marks on the surface along its longitudinal axis.

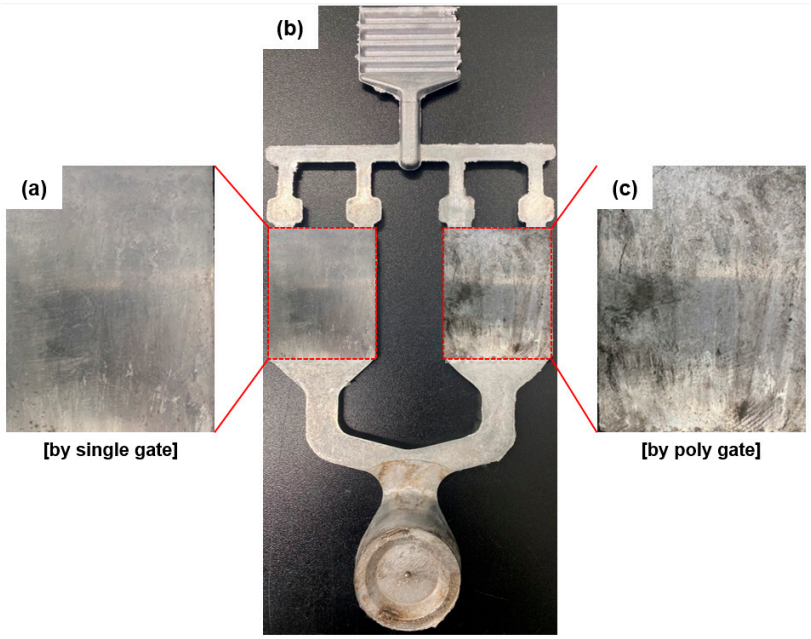


Figure 4. Images of (**b**) as-cast state and (**a**,**c**) cast product of A383 alloy and CNT-added composites cast using a single gate and poly gate using ORDC.

Figure 5 shows the optical microstructures of the A383 alloy cast using a single gate and poly gate using HPDC and ORDC; it shows 0.5–2.0 wt% CNT-added composites cast using a single gate and poly gate using ORDC, respectively. The A383 alloy clearly contains typical microstructural constituents such as the primary α-phase (bright region), Al-Si eutectic Si (darker region) and micropores (Figure 5a,b,g,h). The A383 alloy cast using a poly gate and HPDC (Figure 5g) shows the largest number of micropores, whereas when cast using a using poly gate and ORDC it shows the least amount of micropores (Figure 5h).

The 0.5–2.0 wt% CNT-added composites cast using a single gate and poly gate by using ORDC (Figure 5c–f,i–l) showed some CNT clusters and additional micropores compared to

the A383 alloy cast using a poly gate by using ORDC. Moreover, the amount of micropores tended to increase when using a single gate and increasing the CNT addition.

CNT clustering also tended to increase with the increasing of the CNT addition; the largest clusters were found in the 2.0 wt% CNT-added composites cast using a single gate. The grain sizes in the CNT-added composites were smaller than those in the as-cast A383 alloy, and they tended to be inversely proportional to the added CNT amount.

Electron backscatter diffraction (EBSD) grain size analysis results of the A383 alloy and 1.0 wt% CNT-added composite cast using a single gate and poly gate by using ORDC are shown in Figure 6. The grain sizes of the A383 alloy cast using a single gate and poly gate were 11.38 μm and 10.53 μm, respectively. By contrast, the grain sizes of the 1.0 wt% CNT-added composite cast using a single gate and poly gate were 8.43 μm and 7.05 μm, respectively. The smaller grain size of the 1.0 wt% CNT-added composite compared to that of the A383 alloy was attributed to the added CNTs acting as heterogenous nucleation sites when the molten Al alloy started to solidify and to the grain boundary migration being hindered by the grain boundary pinning effect of the added CNTs by the Zener–Holoman mechanism [28,33]. Furthermore, the grain size of the 1.0 wt% CNT-added composite cast using a poly gate was smaller than that of the composite cast using a single gate; this was attributed to increased nucleation sites with the improved CNT dispersion caused by the poly gate effect.

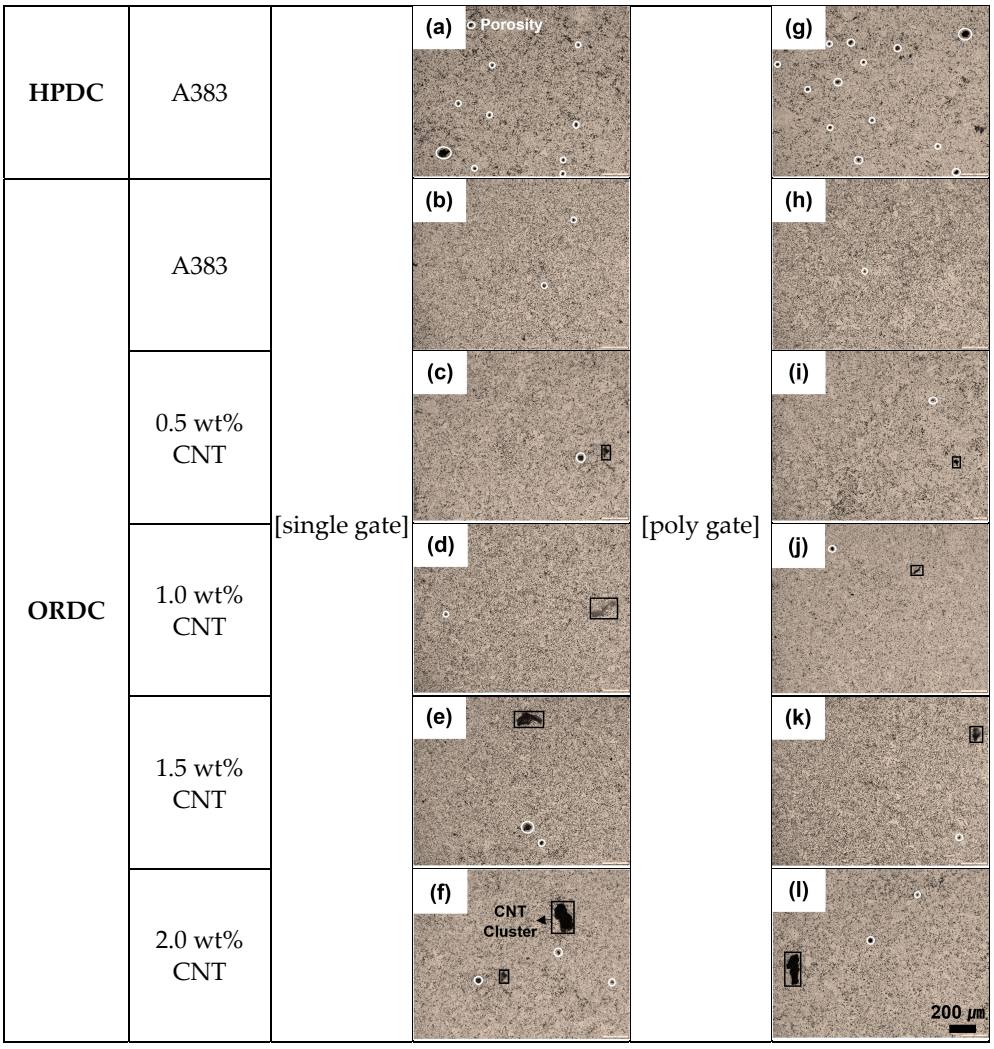


Figure 5. Optical microstructures of A383 alloy cast using a single gate and poly gate by using (**a**,**g**) HPDC and (**b**,**h**) ORDC, respectively; 0.5–2.0 wt% CNT-added composites cast using (**c**–**f**) a single gate and (**i**–**l**) poly gate by using ORDC.

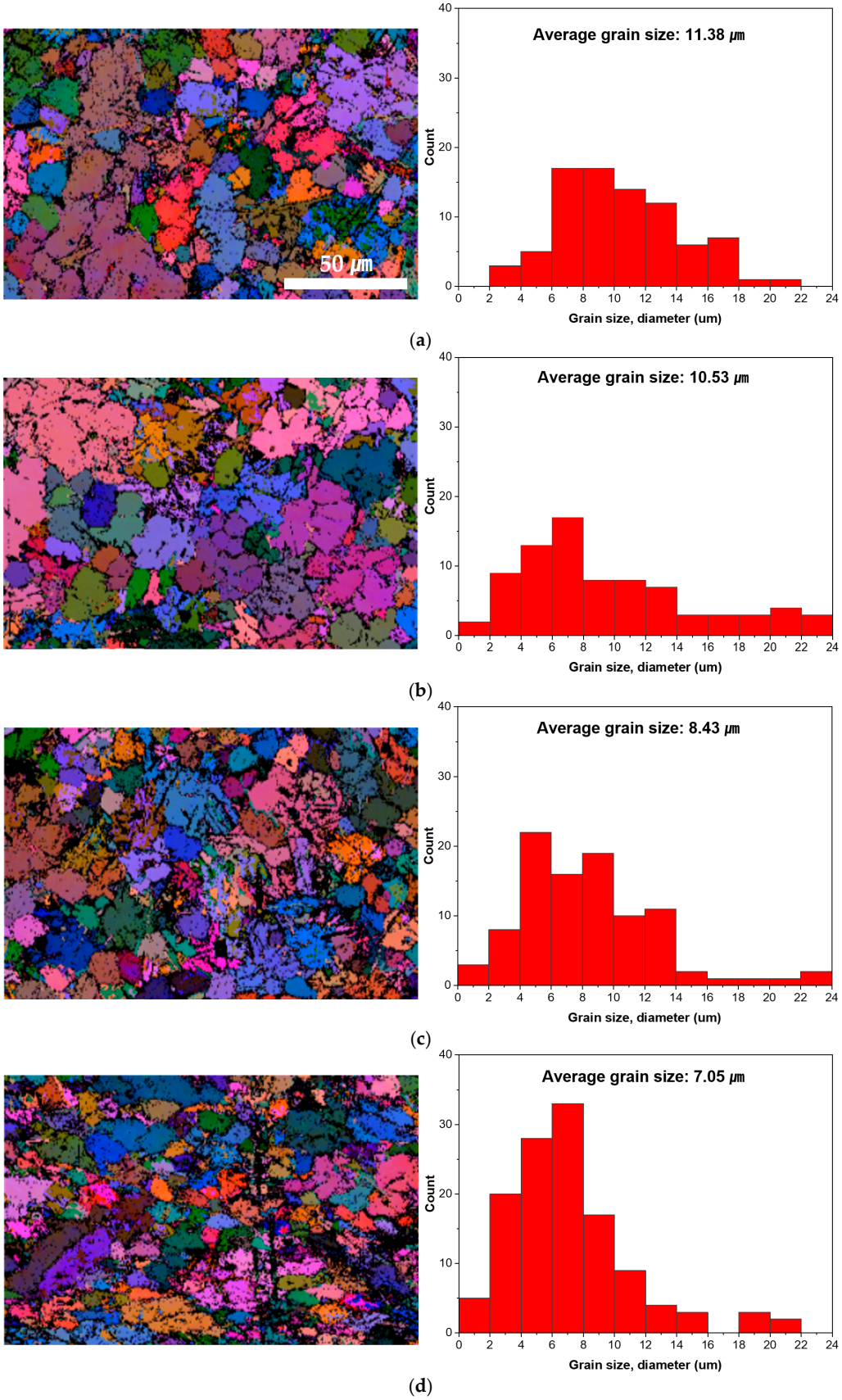


Figure 6. EBSD analysis results of (**a**) A383 alloy cast using a single gate and (**b**) poly gate and (**c**) 1.0 wt% CNT-added composite cast using a single gate and (**d**) poly gate.

Figure 7 shows TEM and SEM images as well as SEM/EDS analysis results for the 1.0 and 2.0 wt% CNT-added composites cast using a poly gate by using ORDC. The TEM images (Figure 7a) show CNTs (d-spacing: ~0.34 nm) and Al_2O_3 (d-spacing: 0.25 nm), respectively, and individual CNTs were around Al_2O_3 owing to the better wettability between Al_2O_3 and CNTs [34,35]. SEM images and SEM/EDS analysis results showed that some CNT clusters with microvoids formed in the matrix of the 1.0 and 2.0 wt% CNT-added composites; the CNT clusters in the former case (Figure 7b) were relatively small in number and individual size (10–20 μm), and those in the latter case (Figure 7e) were larger in number and size (>20 μm). EDS point analysis results for positions P1–P4 corresponding to CNT clusters of the 1.0 and 2.0 wt% CNT-added composites are shown in Figure 7d,g, respectively. Carbon and O_2 as well as constituent elements such as Al, Si and Cu of the A383 alloy were detected, corresponding to the CNT and Al oxide phase, respectively. In particular, the carbon concentration was higher in the 2.0 wt% CNT-added composite than in the 1.0 wt% CNT-added composite, indicating increased CNT aggregation.

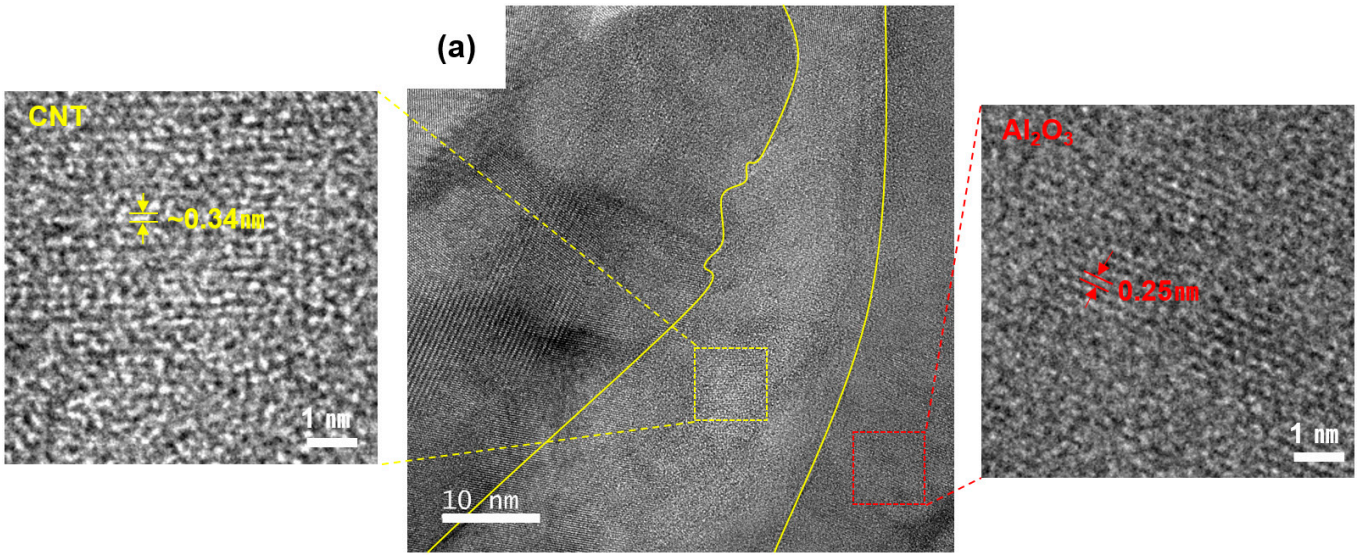
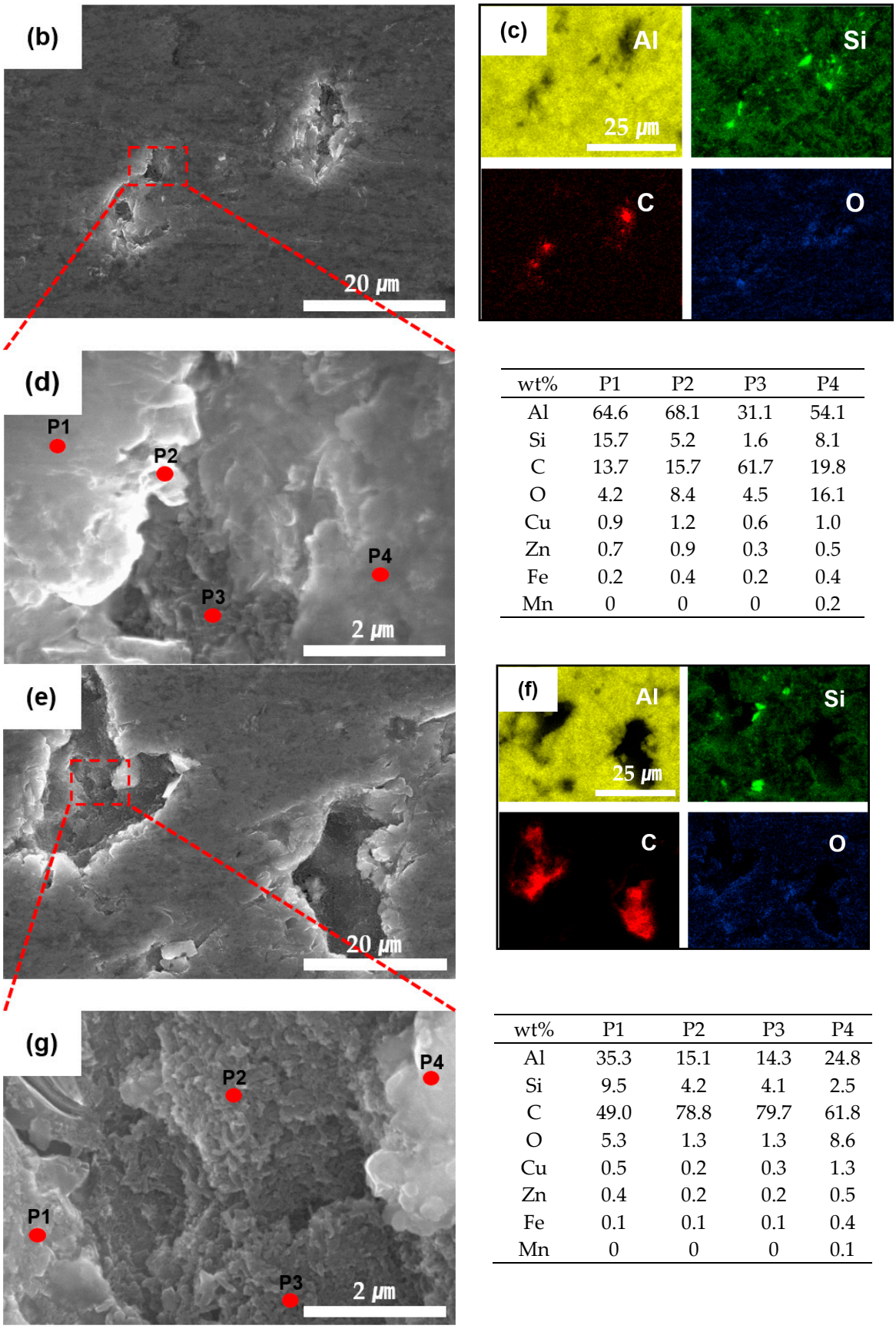


Figure 7. *Cont.*



wt%	P1	P2	P3	P4
Al	64.6	68.1	31.1	54.1
Si	15.7	5.2	1.6	8.1
C	13.7	15.7	61.7	19.8
O	4.2	8.4	4.5	16.1
Cu	0.9	1.2	0.6	1.0
Zn	0.7	0.9	0.3	0.5
Fe	0.2	0.4	0.2	0.4
Mn	0	0	0	0.2

wt%	P1	P2	P3	P4
Al	35.3	15.1	14.3	24.8
Si	9.5	4.2	4.1	2.5
C	49.0	78.8	79.7	61.8
O	5.3	1.3	1.3	8.6
Cu	0.5	0.2	0.3	1.3
Zn	0.4	0.2	0.2	0.5
Fe	0.1	0.1	0.1	0.4
Mn	0	0	0	0.1

Figure 7. (**a**) TEM and (**b**–**d**) SEM images of 1.0 wt% CNT-added composite and (**e**–**g**) SEM images of 2.0 wt% CNT-added composites cast using a poly gate by using ORDC.

3.2. XRD and Raman Spectroscopy Analysis of A383 Alloy and CNT-Added Composite

Figure 8 shows the XRD pattern of the A383 alloy and CNT-added composites. Both showed the Al, Si, SiO_2 and Al_2O_3 phases, but all composites did not show the Al_4C_3 phase, indicating that CNTs were not carbonized during fabrication.

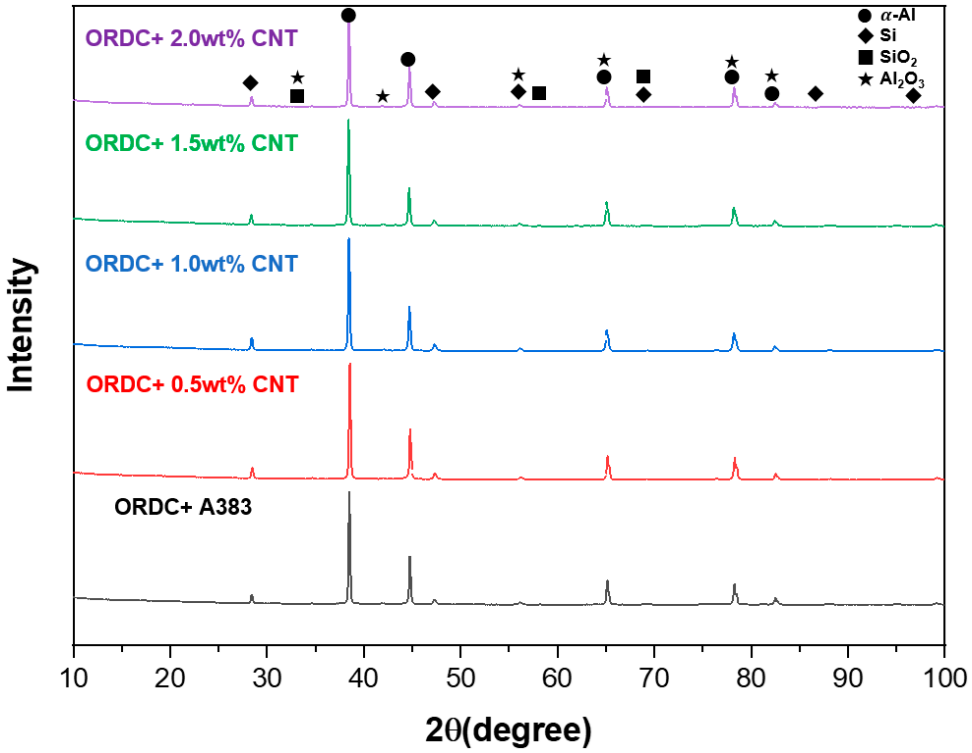


Figure 8. XRD patterns of A383 alloy and 0.5–2.0 wt% CNT-added composites.

Figure 9 shows the Raman spectroscopy analysis results for the composites cast using single and poly gates by using the ORDC process. The intensity ratio (ID/IG) represents the crystal structure damage degree of CNTs, and a higher intensity ratio indicates greater damage of the CNT structure [36–39].

The as-received CNT powder (Figure 9a) showed D and G peaks with values of 1123 and 1024 at ~1344 cm^{-1} and ~1573 cm^{-1}, respectively, indicating that ID/IG = 1.10. The 0.5 and 1.0 wt% CNT-added composites cast using a single gate showed ID/IG values of 1.16 and 1.14, respectively, and those cast using a poly gate showed ID/IG values of 1.13 and 1.14, respectively. These values were not greatly different from those of the as-received CNT powder. Similarly, the 1.5 and 2.0 wt% CNT-added composites cast using a single gate showed ID/IG values of 1.20 and 1.23, respectively, and those cast using a poly gate showed ID/IG values of 1.23 and 1.24, respectively. Slight, but insignificant, damage was confirmed with increasing the CNT addition. Figures 8 and 9 confirmed that the CNTs rarely underwent a carbonization reaction or suffered thermal damage during fabrication by using ORDC as they were exposed to high heat for only a very short time owing to the rapid molten Al filling and solidification.

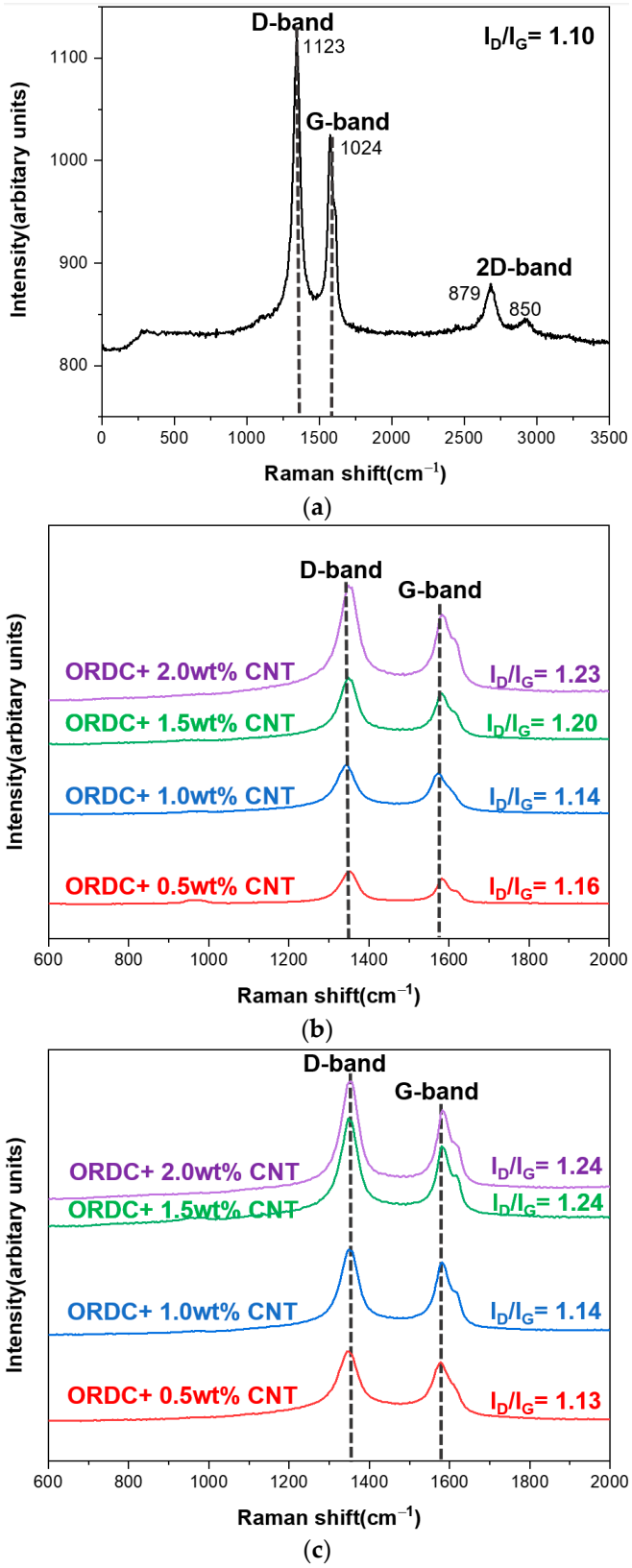


Figure 9. Raman spectroscopy analysis of (**a**) as-received CNTs and 0.5–2.0 wt% CNT-added composites cast using a (**b**) single gate and (**c**) poly gate by using ORDC.

3.3. Porosity Analysis by X-ray CT for A383 Alloy and CNT-Added Composite

X-ray CT inspections were conducted to observe the internal porosities of the A383 alloy and composites cast under various casting conditions; the results are shown in Figure 10. The individual pores had sizes of up to 3 mm^3, and most had sizes of less than 2 mm^3. The total pore volume changed with the CNT addition amount and type of gate used. Internal pores tended to increase with increasing the CNT addition because the spaces between the CNT clusters acted as pores. In ORDC, internal pores reduced significantly when using a poly gate than when using a single gate because the turbulent flow of molten Al when using a poly gate was maximized, thereby increasing the reaction area of molten Al with O_2 and resulting in increased Al_2O_3 formation and decreased residual O_2 gas. By contrast, in HPDC, internal pores increased when using a poly gate than when using a single gate because the turbulent flow of molten Al when using a poly gate was maximized, thereby increasing the pores inside the casting.

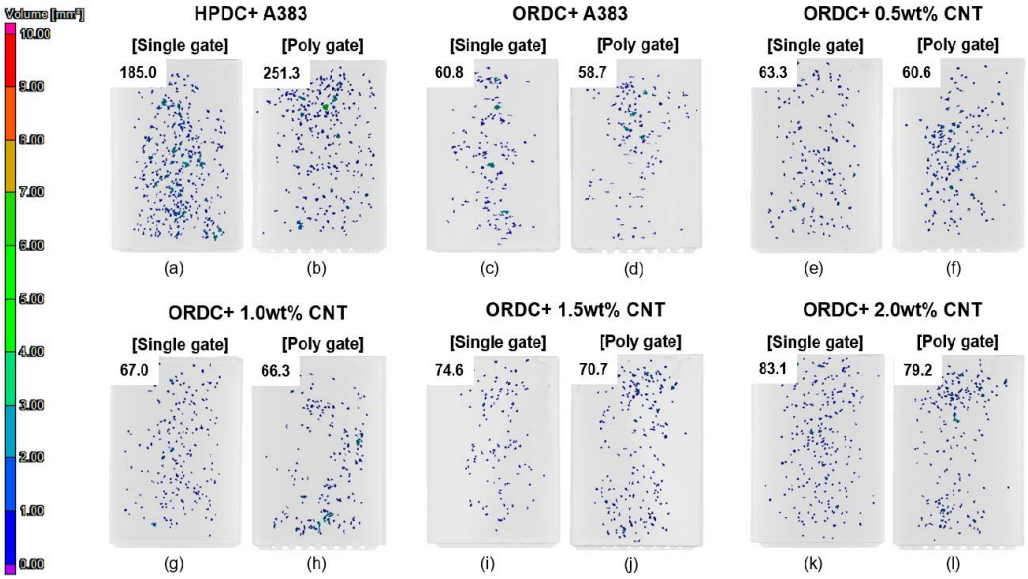
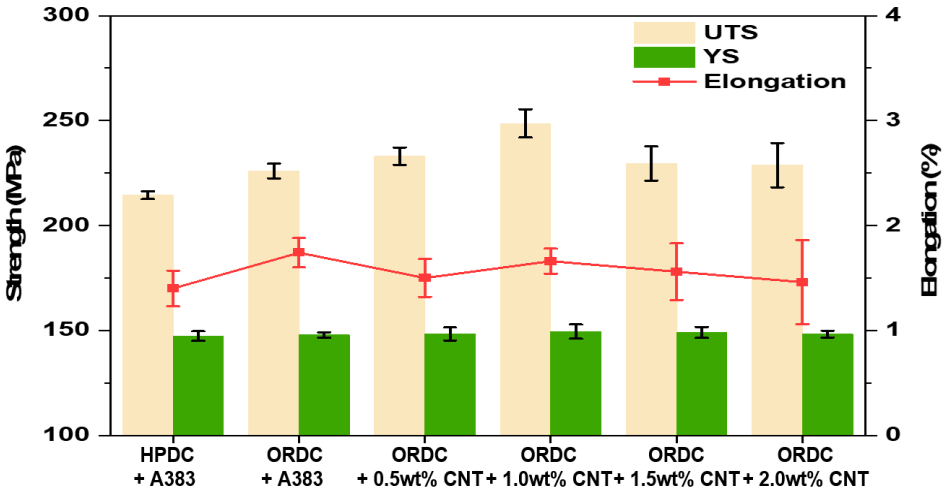


Figure 10. X-ray CT images and porosity analysis of A383 alloy cast using a single gate and poly gate by using (**a**,**b**) HPDC and (**g**,**h**) ORDC, respectively; 0.5–2.0 wt% CNT-added composites cast using (**c**,**e**,**g**,**i**,**k**) a single gate and (**d**,**f**,**h**,**j**,**l**) poly gate by using ORDC.

3.4. Mechanical Properties and Fractographic Examination of CNT-Added Composite

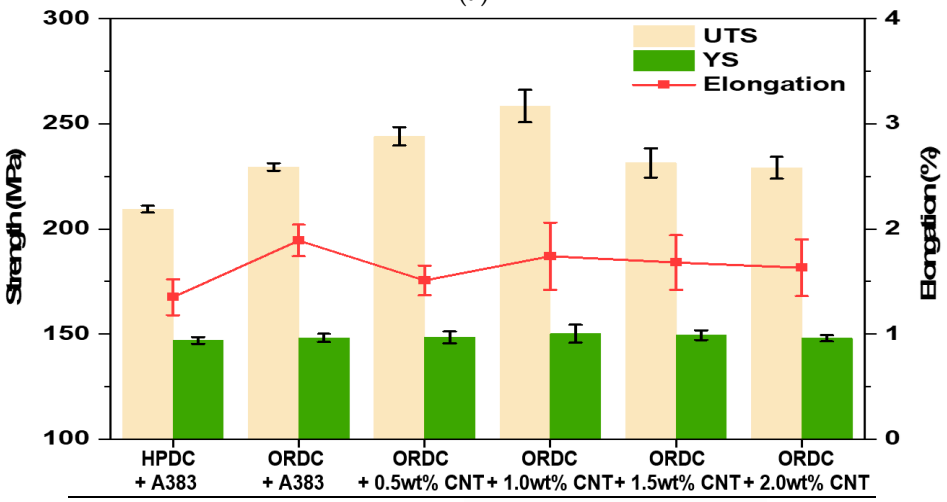
3.4.1. Tensile and Hardness Test

Figure 11 shows the ultimate tensile strength (UTS), yield strength (0.2%YS) and elongation of the A383 alloy and 0.5–2.0 wt% CNT-added composites under various casting conditions with the ORDC and HPDC processes. The tensile strength and yield strength increased with increasing the CNT addition when using a single gate by using ORDC (Figure 11a). The 1.0 wt% CNT-added composite showed a higher average UTS of 248.7 ± 6.6 MPa and YS of 149.4 ± 3.4 MPa compared to those of the as-cast A383 alloy (225.9 ± 1.4 MPa and 147.8 ± 1.3 MPa, respectively). However, the elongation slightly decreased with increasing the CNT addition, resulting in strength enhancement when using a single gate by using ORDC. The 1.0 wt% CNT-added composite showed a slightly lower average elongation of 1.6 ± 0.1% compared to that of the as-cast A383 alloy (1.7 ± 0.1%).



	Standard Deviation (SD)		
	UTS	YS	El
HPDC + A383	1.9	2.3	0.2
ORDC + A383	1.4	1.3	0.1
ORDC + 0.5 wt% CNT	4.1	3.1	0.2
ORDC + 1.0 wt% CNT	6.6	3.4	0.1
ORDC + 1.5 wt% CNT	8.2	2.6	0.3
ORDC + 2.0 wt% CNT	10.6	1.7	0.4

(**a**)



	Standard Deviation (SD)		
	UTS	YS	El
HPDC + A383	1.6	1.6	0.2
ORDC + A383	1.8	1.9	0.2
ORDC + 0.5 wt% CNT	4.4	2.8	0.1
ORDC + 1.0 wt% CNT	5.2	4.2	0.3
ORDC + 1.5 wt% CNT	7.0	2.3	0.3
ORDC + 2.0 wt% CNT	7.7	1.5	0.3

(**b**)

Figure 11. Tensile test results of A383 alloy and 0.5–2.0 wt% CNT-added composites cast using (**a**) a single gate and (**b**) poly gate by using HPDC and ORDC.

The composites cast using a poly gate by using ORDC (Figure 11b) showed a similar change trend of UTS, YS and elongation with CNT addition to those of composites cast using a single gate; however, the absolute UTS value increased in all cases. The 1.0 wt% CNT-added composite cast using a poly gate by using ORDC showed the highest UTS and YS value of 258.5 ± 5.2MPa and 150.1 ± 4.2 MPa, respectively. With HPDC, the UTS, YS and elongation value was lower when using a poly gate than when using a single gate. This was attributed to the increased gas porosity with increased air entrapment due to the enhanced turbulent flow formed when passing through the poly gate in the HPDC process.

The improved mechanical properties of composites cast using a poly gate can be attributed to the improved grain refinement, reduced internal porosities and strong thermal stress at the interface induced by the large difference in the coefficient of thermal expansion between the CNTs and Al matrix. However, a greater than 1.0 wt% CNT addition was found to degrade the tensile strength of the composite to 229.10 ± 7.70 MPa. Generally, clusters of aggregated CNTs are known to degrade the mechanical properties of the composite. The relatively good distribution and low aggregation of CNTs in the 1.0 wt% CNT-added composite were expected to result in superior mechanical properties. However, for the 2.0 wt% CNT-added composite, the large size and numbers of CNT clusters attributable to the flotation and bundling of CNTs owing to the relatively large amount of CNTs degraded the properties of the composite (Figure 7e–g). The lower strength of the 2.0 wt% CNT-added composite may be attributable to increased CNT aggregation and internal porosities induced by the CNT clusters. Therefore, adding more than the optimal amount of CNTs will make the composite more brittle.

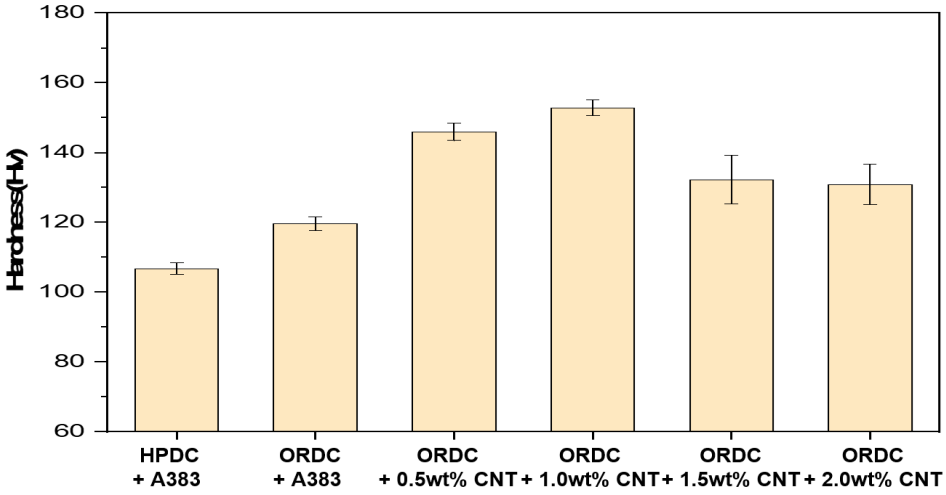
The hardness measurement result of the A383 alloy and 0.5–2.0 wt% CNT-added composites is shown in Figure 12. When using a single gate by using ORDC (Figure 12a), the addition of 1.0, 1.5 and 2.0 wt% CNT resulted in hardness values of 152.8 ± 2.3 Hv, 132.2 ± 7.0 Hv and 130.9 ± 5.7 Hv, respectively; by contrast, the hardness value of the A383 alloy was 119.6 ± 1.9 Hv.

By contrast, when using a poly gate by using ORDC (Figure 12b), 1.0 wt% CNT addition resulted in the highest hardness value of 157.9 ± 3.0 Hv; this was 30% higher than that of the A383 alloy (121.4 ± 2.1 Hv), and the hardness decreased to 136.9 ± 5.8 Hv with 2.0 wt% CNT addition.

As shown above, the UTS and hardness values tended to increase when using a poly gate with up to 1.0 wt% CNT addition in ORDC; this was attributed to the uniform CNT dispersion and improved grain refinement as well as the porosity reduction caused by the improved reactivity between O_2 and molten Al. However, 1.5 and 2.0 wt% CNT addition reduced the UTS and hardness; this was attributed to the porosity formation due to the CNT clusters and the slip between the CNTs clusters under tensile stress [40,41].

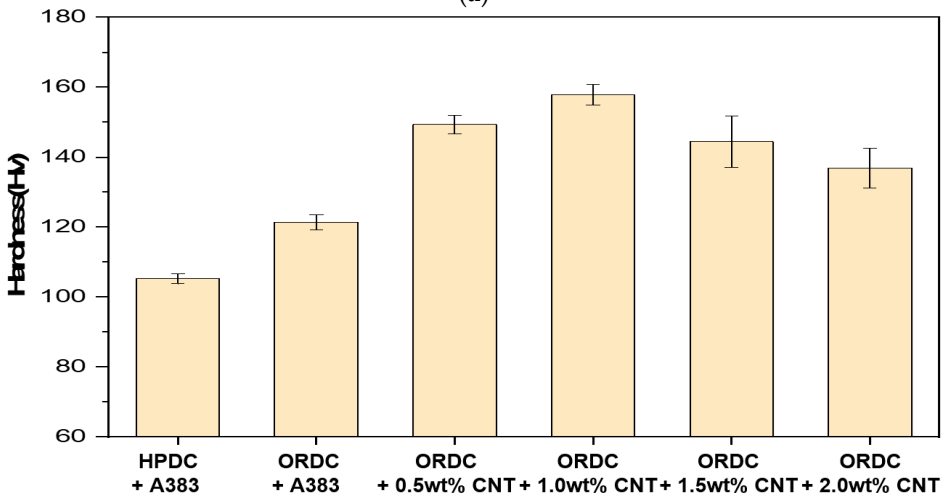
3.4.2. Fractographic Examination

Figure 13 shows fractographic images of the specimens fractured by tensile tests (Figure 11). The 1.0 wt% CNT-added composite cast using pa oly gate (Figure 13a–d) exhibited a large number of dimples with some microvoids that represented a ductile fracture; this was attributed to their better ductility. However, the 2.0 wt% CNT-added composite cast using a poly gate (Figure 13e–h) exhibited cleavage planes with microvoid coalescences associated with brittle fracture. The CNT-added composites have a tendency to become more brittle as CNT clusters increase with the CNT addition amount; this tendency is in good agreement with the trend of the tensile test results shown in Figure 11.



	Standard Deviation (SD)
HPDC + A383	1.7
ORDC + A383	1.9
ORDC + 0.5 wt% CNT	2.5
ORDC + 1.0wt% CNT	2.3
ORDC + 1.5 wt% CNT	7.0
ORDC + 2.0 wt% CNT	5.7

(**a**)



	Standard Deviation (SD)
HPDC + A383	1.4
ORDC + A383	2.1
ORDC + 0.5 wt% CNT	2.6
ORDC + 1.0 wt% CNT	3.0
ORDC + 1.5 wt% CNT	7.4
ORDC + 2.0 wt% CNT	5.8

(**b**)

Figure 12. Vickers hardness of A383 alloy and 0.5–2.0 wt% CNT-added composites cast using (**a**) a single gate and (**b**) poly gate by using HPDC and ORDC.

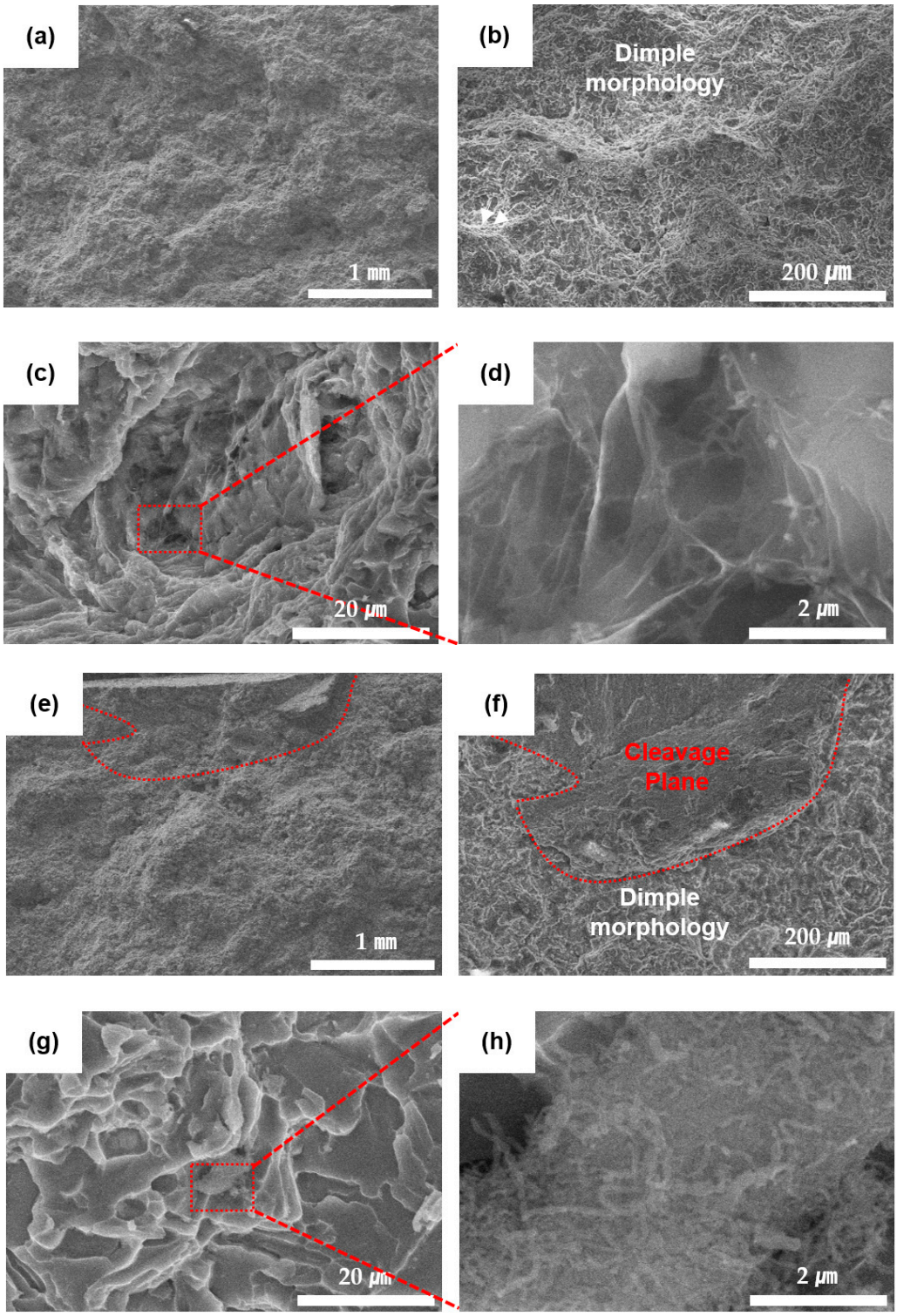


Figure 13. SEM micrographs of fractured surfaces of (**a**–**d**) 1.0 wt% and (**e**–**h**) 2.0 wt% CNT-added composites cast using a poly gate by using ORDC.

Figure 14 shows a schematic of the fabrication of CNT-added composites cast using a single gate and poly gate by using ORDC. First, O_2 was supplied to replace the air (mainly N_2 gas) in the cavity and sleeve; after the air was fully replaced by O_2, CNTs were added into the cavity by the Venturi effect produced by the O_2 supply pressure (Figure 14a,b). Then, molten Al was filled into the cavity with one filling stream pattern formed using a single gate, where it reacted with O_2 to form Al_2O_3 and finally solidified (Figure 14c).

CNTs generally have a relatively large contact angle of 140–160° with Al; thus, they repel each other, resulting in the reduced dispersion of CNTs in Al. However, Al_2O_3 formed by the rapid reaction between molten Al and O_2 gas in ORDC has a relatively low contact angle of ~37° with CNTs; owing to the better wettability between Al_2O_3 and CNTs, CNTs are distributed around Al_2O_3 (Figure 7a), resulting in improved dispersibility of CNTs and grain refinement in the composite [42–44]. Some residual O_2 that did not participate in the Al_2O_3 reaction remained as internal gas porosities, and the small total amount of Al_2O_3 reduced the CNT dispersibility. This left a clustered form and reduced nucleation sites owing to the decrease in CNT dispersion, in turn reducing the grain refinement effect (Figure 14d,e).

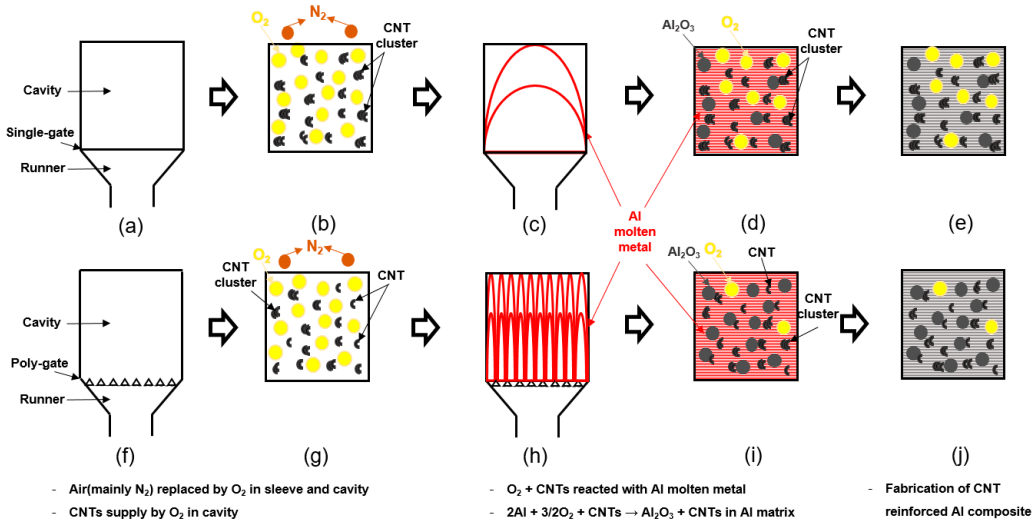


Figure 14. Schematic of fabrication of CNT-added composites cast using (**a**–**e**) a single gate and (**f**–**j**) poly gate by using ORDC.

By contrast, CNTs underwent additional debundling owing to shear stress when they were added into the cavity using a poly gate, as shown in Figure 14f,g. Several melt flow streams occurred when the molten metal flowed into the cavity through the poly gate (Figure 14c,h), as reported in a casting simulation study [45]. The improved reaction area of several turbulent melt flow streams with Al_2O_3 significantly increased Al_2O_3 formation compared to that in the single gate case, resulting in reduced porosities with the reduction of residual O_2. Further, the increased formation of Al_2O_3 that has good wettability with CNTs improved the CNT dispersibility, thus reducing CNT clusters and increasing nucleation sites and consequently improving the grain refinement effect (Figure 14i,j), tensile strength and hardness. However, up to 1.0 wt% CNT addition improved the mechanical properties; 1.5% or 2.0 wt% CNT addition degraded the properties owing to the increase in CNT clusters and internal porosities. Thus, in this study, the 1.0 wt% CNT-added composite cast using a poly gate by using ORDC showed the best CNT dispersion, grain refinement and internal porosities, resulting in the best mechanical properties.

4. Conclusions

In this study, MWCNT-added A383 alloy matrix composites were fabricated by using ORDC with a CNT adding system, and the microstructure and mechanical properties of the composites were evaluated with different CNT adding amounts and gate types. The following conclusions were obtained.

1. As Al molten metal rapidly underwent filling and solidification in ORDC, CNTs were exposed to high heat for a very short time, and therefore, they hardly suffered carbonization or thermal damage.
2. With increasing the CNT addition, CNT clusters increased in the Al matrix. For 1.0 wt% CNT addition using a poly gate, CNT clusters were relatively small, and thus,

CNTs exhibited the best dispersion. The formation of Al_2O_3 that has good wettability with CNTs increased owing to the improved reaction between molten Al and O_2 when using a poly gate.

3. For the same CNT adding amount, grain refinement and internal porosities were lower with the poly gate than with the single gate, owing to the increased nucleation sites with the improved CNT dispersibility and the decreased residual O_2 with the improved reactivity between Al molten metal and O_2 gas.
4. The 1.0 wt% CNT-added composite cast using a poly gate showed the highest UTS of 258.5 ± 5.2 MPa and hardness of 157.9 ± 3.0 Hv. These values were, respectively, 21% and 30% higher than those of the monolithic A383 alloy. This confirmed the feasibility of fabricating the MWCNT-added A383 alloy composite using a poly gate by using ORDC for improved CNT dispersion, grain refinement and reduced internal porosities.

Author Contributions: Conceptualization, S.-H.O. and J.-Y.P.; methodology, P.-H.Y. and J.-Y.P.; validation, S.-H.O., J.-Y.P. and Y.-S.C.; formal analysis, S.-H.O., H.-J.K., P.-H.Y. and G.-H.L.; investigation, S.-H.O., H.-J.K., P.-H.Y., S.-M.S. and G.-H.L.; resources, S.-H.O., H.-J.K., P.-H.Y. and J.-Y.P.; data curation, J.-Y.P., S.-M.S. and Y.-S.C.; writing—original draft preparation, S.-H.O.; writing—review and editing, S.-H.O.; supervision, J.-Y.P. and Y.-S.C.; funding acquisition, J.-Y.P. All authors have read and agreed to the published version of the manuscript.

Funding: This work was supported by the Ministry of Trade, Industry and Energy (code no. P0021899), Republic of Korea.

Institutional Review Board Statement: Not applicable.

Informed Consent Statement: Not applicable.

Data Availability Statement: The data presented in this study are available on request from the corresponding author. The data are not publicly available due to an ongoing study.

Conflicts of Interest: The authors have no conflict of interest.

References

1. Chandel, R.; Sharma, N.; Bansal, S.A. A review on recent developments of aluminum-based hybrid composites for automotive applications. *Emergent Mater.* **2021**, *4*, 1243–1257. [CrossRef]
2. Samal, P.; Tarai, H.; Vundavilli, P.R. Combining effect of annealing and reinforcement content on mechanical behavior of multi-walled CNT reinforced AA5052 composites. *Mater. Today Proc.* **2022**, *62*, 2762–2767. [CrossRef]
3. Tajzad, I.; Ghasali, E. Production methods of CNT-reinforced Al matrix composites: A review. *J. Compos. Compd.* **2020**, *2*, 1–9.
4. Munir, K.S.; Zheng, Y.; Zhang, D.; Lin, J.; Li, Y.; Wen, C. Improving the strengthening efficiency of carbon nanotubes in titanium metal matrix composites. *Mater. Sci. Eng. A* **2017**, *696*, 10–25. [CrossRef]
5. Kondoh, K.; Threrujirapapong, T.; Imai, H.; Umeda, J.; Fugetsu, B. Characteristics of powder metallurgy pure titanium matrix composite reinforced with multi-wall carbon nanotubes. *Compos. Sci. Technol.* **2009**, *69*, 1077–1081. [CrossRef]
6. Xue, F.; Jiehe, S.; Yan, F.; Wei, C. Preparation and elevated temperature compressive properties of multi-walled carbon nanotube reinforced Ti composites. *Mater. Sci. Eng. A* **2010**, *527*, 1586–1589. [CrossRef]
7. Ding, C.; Yu, K.; Nodooshan, H.R.J.; Ye, S.; Yu, P. Effect of powder microstructure on the thermal and mechanical properties of hot extruded Al-CNT composite. *J. Alloys Compd.* **2021**, *891*, 162059. [CrossRef]
8. Zhang, X.; Li, S.; Pan, B.; Pan, D.; Zhou, S.; Yang, S.; Jia, L.; Kondoh, K. A novel strengthening effect of in-situ nano Al_2O_3 on CNTs reinforced aluminum matrix nanocomposites and the matched strengthening mechanisms. *J. Alloys Compd.* **2018**, *764*, 279–288. [CrossRef]
9. Zhang, Z.; Xiao, Y.; Xu, J.; He, M.; Luo, Y.; Xiang, J. Understanding the influencing mechanism of CNTs on the microstructure and mechanical properties of semi-solid stir casting Al-Cu-Mg alloys. *J. Mater. Res. Technol.* **2022**, *18*, 3949–3960. [CrossRef]
10. Carneiro, I.; Simoes, S. Investigation of mechanical properties of Al/CNT nanocomposites produced by powder metallurgy. *Appl. Sci.* **2023**, *13*, 54. [CrossRef]
11. Khasenova, R.S.; Komarov, S.V.; Zadorozhnyy, V.Y. Mechanical plating of Al/CNT composite coatings on aluminum substrates. *J. Alloys Compd.* **2017**, *707*, 238–244. [CrossRef]
12. Dogan, K.; Ozgun, M.; Subutay, H.; Salur, E.; Eker, Y.; Kuntoglu, M.; Aslan, A.; Gupta, M.; Acarer, M. Dispersion mechanism-induced variations in microstructural and mechanical behavior of CNT-reinforced aluminum nanocomposites. *Arch. Civ. Mech. Eng.* **2022**, *22*, 55. [CrossRef]

13. Guo, B.; Song, M.; Zhang, X.; Liu, Y.; Cen, X.; Chen, B.; Li, W. Exploiting the synergic strengthening effects of stacking faults in carbon nanotubes reinforced aluminum matrix composites for enhanced mechanical properties. *Compos. Part B* **2021**, *211*, 108646. [CrossRef]
14. Zeng, M.; Yan, H.; Li, K.; Lei, Y. Microstructure, wettability, and mechanical properties of ADC12 alloy reinforced with TiO_2-coated carbon nanotubes. *J. Alloys Compd.* **2022**, *897*, 163181. [CrossRef]
15. Kumar Tiwari, S.; Singh, H.; Midathada, A.; Sharma, S.; Ravella, U.K. Study of fabrication processes and properties of AL-CNT composites reinforced by carbon nano tubes—A review. *Mater. Today Proc.* **2018**, *5*, 28262–28270. [CrossRef]
16. Fan, G.; Yu, Z.; Tan, Z.; Li, Z.; Zhang, D. Evolution, control, and effects of interface in CNT/Al composites: A review. *Acta Metall. Sin. Engl. Lett.* **2014**, *27*, 839–843. [CrossRef]
17. Noguchi, T.; Magario, A.; Fukazawa, S.; Shimizu, S.; Beppu, J.; Seki, M. Carbon nanotube aluminium composites with uniform dispersion. *Mater. Trans.* **2004**, *45*, 602–604. [CrossRef]
18. Larianovsky, N.; Popov, V.; Katz-Demyanetz, A.; Fleisher, A.; Meyers, D.; Chaudhuri, R. Production of Al metal matrix composites reinforced with carbon nanotubes by two-stage melt-based HPDC-CE method. *J. Eng. Mater. Technol.* **2019**, *141*, 011002. [CrossRef]
19. Eisaabadi, B.G.; Yeom, G.; Tiryakioglu, M.; Netto, N.; Beygi, R.; Mehrizi, M.; SK, K. The effect of solution treatment time on the microstructure and ductility of naturally-aged A383 alloy die castings. *Mater. Sci. Eng. A* **2018**, *722*, 1–7. [CrossRef]
20. Liu, T.; Bunn, J.; Fancher, C.; Nastac, L.; Arvikar, V.; Levin, I.; Brewer, L. Neutron diffraction analysis of residual strain in high-pressure die cast A383 engine blocks. *J. Mater. Eng. Perform.* **2020**, *29*, 5428–5434. [CrossRef]
21. Cai, Q.; Mendis, C.; Chang, I.; Fan, Z. Microstructure evolution and mechanical properties of new die-cast Al-Si-Mg-Mn alloys. *Mater. Des.* **2020**, *187*, 108394. [CrossRef]
22. Koru, M.; Serce, O. The effects of thermal and dynamical parameters and vacuum application on porosity in high-pressure die casting of A383 Al-alloy. *Int. J. Met.* **2018**, *12*, 797–813. [CrossRef]
23. Kang, H.-J.; Yoon, P.-H.; Lee, G.-H.; Park, J.-Y.; Jung, B.-J.; Lee, J.-Y.; Lee, C.-U.; Kim, E.-S.; Choi, Y.-S. Evaluation of the gas porosity and mechanical properties of vacuum assisted pore-free die-cast Al-Si-Cu alloy. *Vacuum* **2021**, *184*, 109917. [CrossRef]
24. Kang, H.-J.; Jang, H.-S.; Oh, S.-H.; Yoon, P.-H.; Lee, G.-H.; Park, J.-Y.; Choi, Y.-S. Effect of injected oxygen amount on the gas porosity and mechanical properties of a pore-free die-cast Al–Si–Cu alloy. *Metals* **2021**, *11*, 1805. [CrossRef]
25. Bar-Meir, G. Analysis of mass transfer process in the pore free technique. *J. Eng. Mater. Technol. Trans. ASME* **1995**, *117*, 215–219. [CrossRef]
26. Kim, E.-S. Special die casting technology. *J. Korean Foundrymen's Soc.* **1997**, *17*, 527–537.
27. Kim, K.-Y.; Yi, M.-S. Progress of the diecasting technology and its application. *J. Korean Foundrymen's Soc.* **1995**, *15*, 339–350.
28. Carneiro, Í.; Simões, S. Strengthening mechanisms in carbon nanotubes reinforced metal matrix composites: A review. *Metals* **2021**, *11*, 1613. [CrossRef]
29. Mohsen, M.; Taha, R.; Taqa, A.; Al-Nuaimi, N.; Al-Rub, R.; Bani-Hani, K. Effect of nanotube geometry on the strength and dispersion of CNT-cement composites. *J. Nanomater.* **2017**, *2017*, 6927416. [CrossRef]
30. Niu, X.P.; Hu, B.H.; Pinwill, I.; Li, H. Vacuum assisted high pressure die casting of aluminium alloys. *J. Mater. Process. Technol.* **2000**, *105*, 119–127. [CrossRef]
31. Bradbury, C.R.; Gomon, J.K.; Kollo, L.; Kwon, H.; Leparoux, M. Hardness of multi wall carbon nanotubes reinforced aluminium matrix composites. *J. Alloys Compd.* **2014**, *585*, 362–367. [CrossRef]
32. Khan, M.; Zulfaqar, M.; Ali, F.; Subhani, T. Microstructural and mechanical characterization of hybrid aluminum matrix composite containing boron carbide and Al-Cu-Fe quasicrystals. *Met. Mater. Int.* **2017**, *23*, 813–822. [CrossRef]
33. Sharma, A.; Fujii, H.; Paul, J. Influence of reinforcement incorporation approach on mechanical and tribological properties of AA6061-CNT nanocomposite fabricated via FSP. *J. Manuf. Process.* **2020**, *59*, 604–620. [CrossRef]
34. Rahman, O.S.A.; Sribalaji, M.; Mukherjee, B.; Laha, T.; Keshri, A.K. Synergistic effect of hybrid carbon nanotube and graphene nanoplatelets reinforcement on processing, microstructure, interfacial stress and mechanical properties of Al_2O_3 nanocomposites. *Ceram. Int.* **2018**, *44*, 2109–2122. [CrossRef]
35. Lin, Z.; Shao, G.; Liu, W.; Wang, Y.; Wang, H.; Wang, H.; Fan, B.; Lu, H.; Xu, H.; Zhang, R. In-situ TEM observations of the structural stability in carbon nanotubes, nanodiamonds and carbon nano-onions under electron irradiation. *Carbon* **2022**, *192*, 356–365. [CrossRef]
36. Usef, A.; Bhajantri, V.; Kannoth, V.; Jambagi, S. Influence of carbon nanotube reinforcement on the heat transfer coefficient, microstructure, and mechanical properties of a die cast Al-7Si-0.35Mg alloy. *J. Alloys Compd.* **2021**, *888*, 160844. [CrossRef]
37. Liu, X.; Li, C.; Eckert, J.; Prashanth, K.; Renk, O.; Teng, L.; Liu, Y.; Bao, R.; Tao, J.; Shen, T.; et al. Microstructure evolution and mechanical properties of carbon nanotubes reinforced Al matrix composites. *Mater. Charact.* **2017**, *133*, 122–132. [CrossRef]
38. Jorio, A.; Saito, R. Raman spectroscopy for carbon nanotube applications. *J. Appl. Phys.* **2021**, *129*, 021102. [CrossRef]
39. Xie, X.; Tan, Z.; Chen, C.; Xie, Y.; Wu, H.; Yan, X.; Gao, S.; Li, Z.; Ji, G.; Liao, H. Synthesis of carbon nanotube reinforced Al matrix composite coatings via cold spray deposition. *Surf. Coat. Technol.* **2021**, *405*, 126676. [CrossRef]
40. Guo, B.; Zhang, X.; Cen, X.; Chen, B.; Wang, X.; Song, M.; Ni, S.; Yi, J.; Shen, T.; Du, Y. Enhanced mechanical properties of aluminum based composites reinforced by chemically oxidized carbon nanotubes. *Carbon* **2018**, *139*, 459–471. [CrossRef]
41. Ming, Z.; Jian, L.; Chunxia, W.; Xiaokang, Z.; Lan, C. Fluid drag reduction on superhydrophobic surfaces coated with carbon nanotube forests (CNTs). *Soft Matter* **2011**, *7*, 4391. [CrossRef]

42. Tjong, S.C. Recent progress in the development and properties of novel metal matrix nanocomposites reinforced with carbon nanotubes and graphene nanosheets. *Mater. Sci. Eng. R* **2013**, *74*, 281–350. [CrossRef]
43. Gupta, A.; Tripathi, G.; Basu, B.; Balani, K. Dependence of protein adsorption on wetting behavior of UHMWPE–HA–Al_2O_3–CNT hybrid biocomposites. *JOM* **2012**, *64*, 506–513. [CrossRef]
44. Balani, K.; Agarwal, A. Wetting of carbon nanotubes by aluminum oxide. *Nanotechnology* **2008**, *19*, 165701. [CrossRef] [PubMed]
45. Kang, H.-J.; Jang, H.-S.; Oh, S.-H.; Yoon, P.-H.; Lee, G.-H.; Shin, S.-M.; Park, J.-Y.; Choi, Y.-S. Effects of gate system design on pore defects and mechanical properties of pore-free die-cast Al-Si-Cu alloy. *Mater. Today Commun.* **2022**, *31*, 103673. [CrossRef]

Disclaimer/Publisher's Note: The statements, opinions and data contained in all publications are solely those of the individual author(s) and contributor(s) and not of MDPI and/or the editor(s). MDPI and/or the editor(s) disclaim responsibility for any injury to people or property resulting from any ideas, methods, instructions or products referred to in the content.